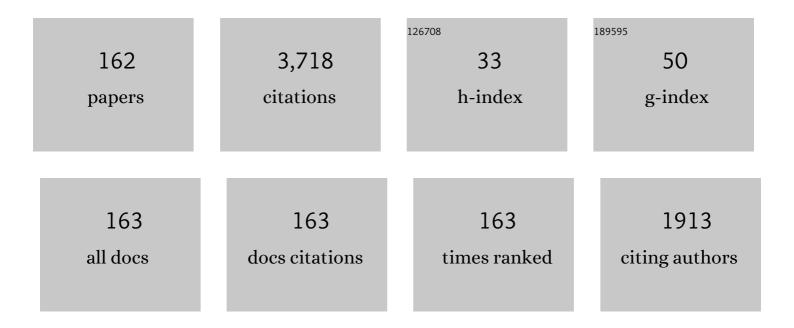
Brian Grierson

List of Publications by Year in descending order

Source: https://exaly.com/author-pdf/439645/publications.pdf Version: 2024-02-01



#	Article	IF	CITATIONS
1	Integrated modeling applications for tokamak experiments with OMFIT. Nuclear Fusion, 2015, 55, 083008.	1.6	246
2	Overview of the JET results in support to ITER. Nuclear Fusion, 2017, 57, 102001.	1.6	150
3	Pedestal Bifurcation and Resonant Field Penetration at the Threshold of Edge-Localized Mode Suppression in the DIII-D Tokamak. Physical Review Letters, 2015, 114, 105002.	2.9	141
4	Enhanced H-mode pedestals with lithium injection in DIII-D. Nuclear Fusion, 2015, 55, 063018.	1.6	123
5	Compatibility of internal transport barrier with steady-state operation in the high bootstrap fraction regime on DIII-D. Nuclear Fusion, 2015, 55, 123025.	1.6	83
6	Efficient generation of energetic ions in multi-ion plasmas by radio-frequency heating. Nature Physics, 2017, 13, 973-978.	6.5	73
7	Active spectroscopic measurements of the bulk deuterium properties in the DIII-D tokamak (invited). Review of Scientific Instruments, 2012, 83, 10D529.	0.6	64
8	Measurements of the deuterium ion toroidal rotation in the DIII-D tokamak and comparison to neoclassical theory. Physics of Plasmas, 2012, 19, .	0.7	62
9	Integrated fusion simulation with self-consistent core-pedestal coupling. Physics of Plasmas, 2016, 23,	0.7	56
10	Improved edge charge exchange recombination spectroscopy in DIII-D. Review of Scientific Instruments, 2016, 87, 11E512.	0.6	54
11	Access to a New Plasma Edge State with High Density and Pressures using the Quiescent <mml:math xmlns:mml="http://www.w3.org/1998/Math/MathML" display="inline"><mml:mi>H</mml:mi>Mode. Physical Review Letters, 2014, 113, 135001.</mml:math 	2.9	53
12	The density dependence of edge-localized-mode suppression and pump-out by resonant magnetic perturbations in the DIII-D tokamak. Physics of Plasmas, 2019, 26, .	0.7	51
13	High fusion performance in Super H-mode experiments on Alcator C-Mod and DIII-D. Nuclear Fusion, 2019, 59, 086017.	1.6	48
14	Impurity confinement and transport in high confinement regimes without edge localized modes on	0.7	47
15	Non-perturbative measurement of cross-field thermal diffusivity reduction at the O-point of 2/1 neoclassical tearing mode islands in the DIII-D tokamak. Physics of Plasmas, 2016, 23, .	0.7	46
16	The quiescent H-mode regime for high performance edge localized mode-stable operation in future	0.7	45
17	The effect of the fast-ion profile on Alfvén eigenmode stability. Nuclear Fusion, 2013, 53, 093006.	1.6	44
18	Orchestrating TRANSP Simulations for Interpretative and Predictive Tokamak Modeling with OMFIT. Fusion Science and Technology, 2018, 74, 101-115.	0.6	44

#	Article	IF	CITATIONS
19	Confinement degradation by Alfvén-eigenmode induced fast-ion transport in steady-state scenario discharges. Plasma Physics and Controlled Fusion, 2014, 56, 095030.	0.9	43
20	Validation of the model for ELM suppression with 3D magnetic fields using low torque ITER baseline scenario discharges in DIII-D. Physics of Plasmas, 2017, 24, .	0.7	43
21	Fast ion transport during applied 3D magnetic perturbations on DIII-D. Nuclear Fusion, 2015, 55, 073028.	1.6	42
22	High frequency pacing of edge localized modes by injection of lithium granules in DIII-D H-mode discharges. Nuclear Fusion, 2016, 56, 056008.	1.6	42
23	OMFIT Tokamak Profile Data Fitting and Physics Analysis. Fusion Science and Technology, 2018, 74, 125-134.	0.6	42
24	Neural-network accelerated coupled core-pedestal simulations with self-consistent transport of impurities and compatible with ITER IMAS. Nuclear Fusion, 2021, 61, 026006.	1.6	42
25	Wide Operational Windows of Edge-Localized Mode Suppression by Resonant Magnetic Perturbations in the DIII-D Tokamak. Physical Review Letters, 2020, 125, 045001.	2.9	40
26	Improved core-edge compatibility using impurity seeding in the small angle slot (SAS) divertor at DIII-D. Physics of Plasmas, 2020, 27, .	0.7	39
27	055904.	0.7	38
28	Main ion and impurity edge profile evolution across the L- to H-mode transition on DIII-D. Plasma Physics and Controlled Fusion, 2018, 60, 105001.	0.9	38
29	Super H-mode: theoretical prediction and initial observations of a new high performance regime for tokamak operation. Nuclear Fusion, 2015, 55, 083026.	1.6	36
30	The role of edge resonant magnetic perturbations in edge-localized-mode suppression and density pump-out in low-collisionality DIII-D plasmas. Nuclear Fusion, 2020, 60, 076001.	1.6	36
31	Energetic ion transport by microturbulence is insignificant in tokamaks. Physics of Plasmas, 2013, 20, 056108.	0.7	35
32	Identifying the location of the OMP separatrix in DIII-D using power accounting. Nuclear Fusion, 2015, 55, 093014.	1.6	35
33	Grassy-ELM regime with edge resonant magnetic perturbations in fully noninductive plasmas in the DIII-D tokamak. Nuclear Fusion, 2018, 58, 106010.	1.6	35
34	Collisionality scaling of main-ion toroidal and poloidal rotation in low torque DIII-D plasmas. Nuclear Fusion, 2013, 53, 063010.	1.6	34
35	Kinetic neoclassical transport in the H-mode pedestal. Physics of Plasmas, 2014, 21, .	0.7	34
36	Gyrokinetic predictions of multiscale transport in a DIII-D ITER baseline discharge. Nuclear Fusion, 2017, 57, 066043.	1.6	34

#	Article	IF	CITATIONS
37	Predicting rotation for ITER via studies of intrinsic torque and momentum transport in DIII-D. Physics of Plasmas, 2017, 24, .	0.7	34
38	Explaining Cold-Pulse Dynamics in Tokamak Plasmas Using Local Turbulent Transport Models. Physical Review Letters, 2018, 120, 075001.	2.9	34
39	Active spectroscopy measurements of the deuterium temperature, rotation, and density from the core to scrape off layer on the DIII-D tokamak (invited). Review of Scientific Instruments, 2018, 89, 10D110.	0.6	34
40	Role of density gradient driven trapped electron mode turbulence in the H-mode inner core with electron heating. Physics of Plasmas, 2016, 23, 056112.	0.7	33
41	Progress toward steady-state tokamak operation exploiting the high bootstrap current fraction regime. Physics of Plasmas, 2016, 23, .	0.7	33
42	Joint DIII-D/EAST research on the development of a high poloidal beta scenario for the steady state missions of ITER and CFETR. Plasma Physics and Controlled Fusion, 2018, 60, 014043.	0.9	32
43	Testing predictions of electron scale turbulent pedestal transport in two DIII-D ELMy H-modes. Nuclear Fusion, 2021, 61, 056005.	1.6	30
44	Main-Ion Intrinsic Toroidal Rotation Profile Driven by Residual Stress Torque from Ion Temperature Gradient Turbulence in the DIII-D Tokamak. Physical Review Letters, 2017, 118, 015002.	2.9	28
45	Intrinsic rotation produced by ion orbit loss and X-loss. Physics of Plasmas, 2012, 19, .	0.7	27
46	The role of zonal flows and predator–prey oscillations in triggering the formation of edge and core transport barriers. Nuclear Fusion, 2014, 54, 073012.	1.6	27
47	Experimental evidence of edge intrinsic momentum source driven by kinetic ion loss and edge radial electric fields in tokamaks. Physics of Plasmas, 2016, 23, 092506.	0.7	27
48	Access to high beta advanced inductive plasmas at low injected torque. Nuclear Fusion, 2013, 53, 093033.	1.6	25
49	Advances in the steady-state hybrid regime in DIII-D—a fully non-inductive, ELM-suppressed scenario for ITER. Nuclear Fusion, 2017, 57, 116057.	1.6	25
50	Turbulence and sheared flow structures behind the isotopic dependence of the L-H power threshold on DIII-D. Nuclear Fusion, 2017, 57, 126015.	1.6	25
51	Progress and challenges in understanding core transport in tokamaks in support to ITER operations. Plasma Physics and Controlled Fusion, 2020, 62, 014021.	0.9	25
52	Deuterium velocity and temperature measurements on the DIII-D tokamak. Review of Scientific Instruments, 2010, 81, 10D735.	0.6	24
53	High resolution main-ion charge exchange spectroscopy in the DIII-D H-mode pedestal. Review of Scientific Instruments, 2016, 87, 11E545.	0.6	24
54	Measurement of deuterium density profiles in the H-mode steep gradient region using charge exchange recombination spectroscopy on DIII-D. Review of Scientific Instruments, 2016, 87, 11E553.	0.6	24

#	Article	IF	CITATIONS
55	Formation of a High Pressure Staircase Pedestal with Suppressed Edge Localized Modes in the DIII-D Tokamak. Physical Review Letters, 2019, 123, 115001.	2.9	24
56	Validation studies of gyrofluid and gyrokinetic predictions of transport and turbulence stiffness using the DIII-D tokamak. Nuclear Fusion, 2013, 53, 083027.	1.6	22
57	Improved confinement in highly powered high performance scenarios on DIII-D. Nuclear Fusion, 2017, 57, 086004.	1.6	22
58	Main-ion intrinsic toroidal rotation across the ITG/TEM boundary in DIII-D discharges during ohmic and electron cyclotron heating. Physics of Plasmas, 2019, 26, 042304.	0.7	22
59	Interpretation of rotation and momentum transport in the DIII-D edge plasma and comparison with neoclassical theory. Nuclear Fusion, 2014, 54, 073021.	1.6	21
60	Particle transport in low-collisionality H-mode plasmas on DIII-D. Nuclear Fusion, 2015, 55, 113025.	1.6	20
61	Exploration of the Super H-mode regime on DIII-D and potential advantages for burning plasma devices. Physics of Plasmas, 2016, 23, .	0.7	20
62	Advances in the high bootstrap fraction regime on DIII-D towards the <i>Q</i> =  5 mission of state. Nuclear Fusion, 2017, 57, 056008.	ITER stead	ly ₂₀
63	Improving fast-ion confinement in high-performance discharges by suppressing Alfvén eigenmodes. Nuclear Fusion, 2017, 57, 056024.	1.6	20
64	Predicting operational windows of ELMs suppression by resonant magnetic perturbations in the DIII-D and KSTAR tokamaks. Physics of Plasmas, 2021, 28, .	0.7	20
65	Impact of toroidal and poloidal mode spectra on the control of non-axisymmetric fields in tokamaks. Physics of Plasmas, 2017, 24, .	0.7	19
66	Calculation of impurity poloidal rotation from measured poloidal asymmetries in the toroidal rotation of a tokamak plasma. Review of Scientific Instruments, 2012, 83, 10D501.	0.6	18
67	Rotation profile flattening and toroidal flow shear reversal due to the coupling of magnetic islands in tokamaks. Physics of Plasmas, 2016, 23, 056107.	0.7	18
68	Multi-scale transport in the DIII-D ITER baseline scenario with direct electron heating and projection to ITER. Physics of Plasmas, 2018, 25, .	0.7	18
69	Analysis of deposited layers with deuterium and impurity elements on samples from the divertor of JET with ITER-like wall. Journal of Nuclear Materials, 2019, 516, 202-213.	1.3	18
70	Understanding LOC/SOC phenomenology in tokamaks. Nuclear Fusion, 2020, 60, 105001.	1.6	18
71	Initial measurements of the DIII-D off-axis neutral beams. Nuclear Fusion, 2012, 52, 094005.	1.6	17
72	Dependence of intrinsic torque and momentum confinement on normalized gyroradius and collisionality in the DIII-D tokamak. Physics of Plasmas, 2017, 24, 042501.	0.7	17

#	Article	IF	CITATIONS
73	Control of power, torque, and instability drive using in-shot variable neutral beam energy in tokamaks. Nuclear Fusion, 2017, 57, 014001.	1.6	17
74	Dynamic neutral beam current and voltage control to improve beam efficacy in tokamaks. Physics of Plasmas, 2018, 25, .	0.7	17
75	Alfvén eigenmodes and fast ion transport in negative triangularity DIII-D plasmas. Nuclear Fusion, 2019, 59, 086028.	1.6	17
76	Comparison of the numerical modelling and experimental measurements of DIII-D separatrix displacements during H-modes with resonant magnetic perturbations. Nuclear Fusion, 2014, 54, 093008.	1.6	16
77	Control of plasma stored energy for burn control using DIII-D in-vessel coils. Nuclear Fusion, 2015, 55, 053001.	1.6	16
78	Suppression of type-I ELMs with reduced RMP coil set on DIII-D. Nuclear Fusion, 2016, 56, 036020.	1.6	16
79	Predicting the rotation profile in ITER. Nuclear Fusion, 2020, 60, 036003.	1.6	16
80	Design and physics basis for the upcoming DIII-D SAS-VW campaign to quantify tungsten leakage and transport in a new slot divertor geometry. Physica Scripta, 2021, 96, 124073.	1.2	16
81	Impurity leakage and radiative cooling in the first nitrogen and neon seeding study in the closed DIII-D SAS configuration. Nuclear Fusion, 2022, 62, 026021.	1.6	16
82	Thermal ion orbit loss and radial electric field in DIII-D. Physics of Plasmas, 2015, 22, 080701.	0.7	15
83	On the very high energy confinement observed in super H-mode DIII-D experiments. Nuclear Fusion, 2020, 60, 034001.	1.6	15
84	Predict-first experiments and modeling of perturbative cold pulses in the DIII-D tokamak. Physics of Plasmas, 2019, 26, .	0.7	14
85	Shattered pellet penetration in low and high energy plasmas on DIII-D. Nuclear Fusion, 2020, 60, 036014.	1.6	14
86	On the stability and stationarity of the Super H-mode combined with an ion transport barrier in the core. Plasma Physics and Controlled Fusion, 2021, 63, 025017.	0.9	14
87	Testing neoclassical and turbulent effects on poloidal rotation in the core of DIII-D. Physics of Plasmas, 2014, 21, .	0.7	13
88	Optimizing the Super H-mode pedestal to improve performance and facilitate divertor integration. Physics of Plasmas, 2020, 27, 102506.	0.7	13
89	Localized divertor leakage measurements using isotopic tungsten sources during edge-localized mode-y H-mode discharges on DIII-D. Nuclear Fusion, 2020, 60, 016028.	1.6	13
90	Creation and sustainment of wide pedestal quiescent H-mode with zero net neutral beam torque. Nuclear Fusion, 2020, 60, 086005.	1.6	13

#	Article	IF	CITATIONS
91	Fusion pilot plant performance and the role of a sustained high power density tokamak. Nuclear Fusion, 2022, 62, 036026.	1.6	13
92	Global and local characterization of turbulent and chaotic structures in a dipole-confined plasma. Physics of Plasmas, 2009, 16, 055902.	0.7	12
93	Extending the physics basis of quiescent H-mode toward ITER relevant parameters. Nuclear Fusion, 2015, 55, 073031.	1.6	12
94	The energy confinement response of DIII-D plasmas to resonant magnetic perturbations. Nuclear Fusion, 2017, 57, 116030.	1.6	12
95	Perturbative transport modeling of cold-pulse dynamics in Alcator C-Mod Ohmic plasmas. Nuclear Fusion, 2019, 59, 066017.	1.6	12
96	The dominant micro-turbulence instabilities in the lower <i>q</i> ₉₅ high <i>β</i> _p plasmas on DIII-D and predict-first extrapolation. Nuclear Fusion, 2020, 60, 016023.	1.6	12
97	Setting the H-mode pedestal structure: variations of particle source location using gas puff and pellet fueling. Nuclear Fusion, 2020, 60, 046003.	1.6	12
98	Real-time pedestal optimization and ELM control with 3D fields and gas flows on DIII-D. Nuclear Fusion, 2020, 60, 076004.	1.6	12
99	Examination of stiff ion temperature gradient mode physics in simulations of DIII-D H-mode transport. Nuclear Fusion, 2021, 61, 066033.	1.6	12
100	Resolving the mystery of transport within internal transport barriers. Physics of Plasmas, 2014, 21, 055902.	0.7	11
101	Experimental challenges to stiffness as a transport paradigm. Nuclear Fusion, 2018, 58, 026023.	1.6	11
102	Deuterium charge exchange recombination spectroscopy from the top of the pedestal to the scrape off layer in H-mode plasmas. Journal of Instrumentation, 2017, 12, C10013-C10013.	0.5	11
103	DIII-D research advancing the physics basis for optimizing the tokamak approach to fusion energy. Nuclear Fusion, 2022, 62, 042024.	1.6	11
104	Response of impurity particle confinement time to external actuators in QH-mode plasmas on DIII-D. Nuclear Fusion, 2014, 54, 114011.	1.6	10
105	Magnetic shear effects on plasma transport and turbulence at high electron to ion temperature ratio in DIII-D and JT-60U plasmas. Nuclear Fusion, 2017, 57, 056027.	1.6	10
106	Understanding and predicting profile structure and parametric scaling of intrinsic rotation. Physics of Plasmas, 2017, 24, 092501.	0.7	10
107	Expanding the parameter space of the wide-pedestal QH-mode towards ITER conditions. Nuclear Fusion, 2020, 60, 092006.	1.6	10
108	3D modeling of boron transport in DIII-D L-mode wall conditioning experiments. Nuclear Materials and Energy, 2021, 26, 100900.	0.6	10

7

#	Article	IF	CITATIONS
109	ELM suppression in helium plasmas with 3D magnetic fields. Nuclear Fusion, 2017, 57, 086016.	1.6	9
110	A path to stable low-torque plasma operation in ITER with test blanket modules. Nuclear Fusion, 2017, 57, 036004.	1.6	9
111	Simulation of density fluctuations before the L-H transition for Hydrogen and Deuterium plasmas in the DIII-D tokamak using the BOUT++ code. Nuclear Fusion, 2018, 58, 026026.	1.6	9
112	Validation of the kinetic-turbulent-neoclassical theory for edge intrinsic rotation in DIII-D. Physics of Plasmas, 2018, 25, 056114.	0.7	9
113	Observation of fully detached divertor integrated with improved core confinement for tokamak fusion plasmas. Physics of Plasmas, 2021, 28, .	0.7	9
114	Impurity transport in the pedestal of H-mode plasmas with resonant magnetic perturbations. Plasma Physics and Controlled Fusion, 2020, 62, 095021.	0.9	9
115	Ion thermal transport in the H-mode edge transport barrier on DIII-D. Physics of Plasmas, 2022, 29, .	0.7	9
116	Comparison of measured impurity poloidal rotation in DIII-D with neoclassical predictions under low toroidal field conditions. Nuclear Fusion, 2014, 54, 083020.	1.6	8
117	High performance double-null plasmas under radiating divertor and mantle scenarios on DIII-D. Nuclear Fusion, 2019, 59, 086053.	1.6	8
118	Transport Induced by Large Scale Convective Structures in a Dipole-Confined Plasma. Physical Review Letters, 2010, 105, 205004.	2.9	7
119	Alfvén eigenmode structure during off-axis neutral beam injection. Nuclear Fusion, 2012, 52, 103009.	1.6	7
120	Determination of neutral beam energy fractions from collisional radiative measurements on DIII-D. Review of Scientific Instruments, 2012, 83, 10D518.	0.6	7
121	Measurements of fast-ion transport by mode-particle resonances on DIII-D. Nuclear Fusion, 2012, 52, 103022.	1.6	7
122	Manifestations of the geodesic acoustic mode driven by energetic ions in tokamaks. Plasma Physics and Controlled Fusion, 2016, 58, 045024.	0.9	7
123	Feedback control of stored energy and rotation with variable beam energy and perveance on DIII-D. Nuclear Fusion, 2019, 59, 076004.	1.6	7
124	Pedestal collapse by resonant magnetic perturbations. Nuclear Fusion, 2021, 61, 044001.	1.6	7
125	Evolution of ELMs, pedestal profiles and fluctuations in the inter-ELM period in NBI- and ECH-dominated discharges in DIII-D. Nuclear Fusion, 2021, 61, 056008.	1.6	7
126	Nonlinear two-fluid modeling of plasma response to RMPs for the ELM control in the ITER baseline. Nuclear Fusion, 2021, 61, 106006.	1.6	7

#	Article	IF	CITATIONS
127	Testing the DIII-D co/counter off-axis neutral beam injected power and ability to balance injected torque. Nuclear Fusion, 0, , .	1.6	7
128	Kinetic theory and atomic physics corrections for determination of ion velocities from charge-exchange spectroscopy. Nuclear Fusion, 2013, 53, 093012.	1.6	6
129	Phase-locking of magnetic islands diagnosed by ECE-imaging. Review of Scientific Instruments, 2014, 85, 11D847.	0.6	6
130	A method for determining poloidal rotation from poloidal asymmetry in toroidal rotation (invited). Review of Scientific Instruments, 2014, 85, 11E302.	0.6	6
131	Synergy between fast-ion transport by core MHD and test blanket module fields in DIII-D experiments. Nuclear Fusion, 2015, 55, 083023.	1.6	6
132	High-performance double-null plasmas under radiating mantle scenarios on DIII-D. Nuclear Materials and Energy, 2019, 19, 267-272.	0.6	6
133	H-mode pedestal improvements with neon injection in DIII-D. Nuclear Fusion, 2020, 60, 056013.	1.6	6
134	Calibration techniques for fast-ion DÎ \pm diagnostics. Review of Scientific Instruments, 2012, 83, 10D903.	0.6	5
135	High speed measurements of neutral beam turn-on and impact of beam modulation on measurements of ion density. Review of Scientific Instruments, 2014, 85, 103502.	0.6	5
136	Improved kinetic neoclassical transport calculation for a low-collisionality QH-mode pedestal. Plasma Physics and Controlled Fusion, 2016, 58, 085009.	0.9	5
137	Enhanced helium exhaust during edge-localized mode suppression by resonant magnetic perturbations at DIII-D. Nuclear Fusion, 2020, 60, 054004.	1.6	5
138	Relative intensity calibration of the DIII-D charge-exchange recombination spectroscopy system using neutral beam injection into gas. Review of Scientific Instruments, 2018, 89, 10D116.	0.6	4
139	Response of thermal and fast-ion transport to beam ion population, rotation and T _e /T _i in the DIII-D steady state hybrid scenario. Nuclear Fusion, 2021, 61, 036036.	1.6	4
140	Radially resolved active charge exchange measurements of the hydrogenic isotope fraction on DIII-D. Review of Scientific Instruments, 2021, 92, 043535.	0.6	4
141	The role of toroidal rotation in the very high energy confinement quality observed in super H-mode experiments on DIII-D. Physics of Plasmas, 2021, 28, .	0.7	4
142	Spatial calibration of a tokamak neutral beam diagnostic using in situ neutral beam emission. Review of Scientific Instruments, 2015, 86, 103509.	0.6	3
143	Application of ECH to the Study of Transport in ITER Baseline Scenario-like Discharges in DIII-D. EPJ Web of Conferences, 2015, 87, 02003.	0.1	3
144	The effect of electron cyclotron heating on density fluctuations at ion and electron scales in ITER baseline scenario discharges on the DIII-D tokamak. Nuclear Fusion, 2017, 57, 126014.	1.6	3

#	Article	IF	CITATIONS
145	A computational tool for simulation and design of tangential multi-energy soft x-ray pin-hole cameras for tokamak plasmas. Review of Scientific Instruments, 2018, 89, 10G120.	0.6	3
146	Using motional Stark splitting of Dα emission to constrain MHD equilibrium analysis in DIII-D plasmas. Review of Scientific Instruments, 2018, 89, 10D111.	0.6	3
147	Synthetic diagnostic for assessing spatial averaging of charge exchange recombination spectroscopy measurements. Review of Scientific Instruments, 2018, 89, 10D101.	0.6	3
148	Safety factor and turbulence dynamics dependence of the L-H power threshold on DIII-D. Physics of Plasmas, 2019, 26, 062507.	0.7	3
149	Deconvolving the roles of E × B shear and pedestal structure in the energy confinement quality of super H-mode experiments. Nuclear Fusion, 2022, 62, 056008.	1.6	3
150	Numerical modeling of pedestal stability and broadband turbulence of wide-pedestal QH-mode plasmas on DIII-D. Nuclear Fusion, 2022, 62, 076033.	1.6	3
151	Fast wave direct electron heating in advanced inductive and ITER baseline scenario discharges in DIII-D. , 2014, , .		2
152	Impact of central ECCD on steady-state hybrid scenario in DIII-D. AIP Conference Proceedings, 2015, , .	0.3	2
153	Integrated Zeff analysis on the DIII-D Tokamak. Journal of Instrumentation, 2019, 14, C10002-C10002.	0.5	2
154	Development of an integrated core–edge scenario using the super H-mode. Nuclear Fusion, 2021, 61, 126064.	1.6	2
155	Understanding the core confinement in DIII-D super-H experiments by transport modeling. Nuclear Fusion, 2022, 62, 086017.	1.6	2
156	Electron cyclotron heating and core intrinsic rotation reversal in DIII-D. AIP Conference Proceedings, 2015, , .	0.3	1
157	DIII-D shaping demonstrates correlation of intrinsic momentum with energy. Nuclear Fusion, 2019, 59, 096011.	1.6	1
158	Explaining the lack of power degradation of energy confinement in wide pedestal quiescent H-modes via transport modeling. Nuclear Fusion, 2022, 62, 056024.	1.6	1
159	Enhanced localized energetic ion losses resulting from first-orbit linear and non-linear interactions with Alfvén eigenmodes in DIII-D. Physics of Plasmas, 2014, 21, 082503.	0.7	0
160	Propagation of input parameter uncertainties in transport models. Physics of Plasmas, 2018, 25, .	0.7	0
161	Charge exchange recombination spectroscopy measurements of DIII-D poloidal rotation with poloidal asymmetry in angular rotation. Review of Scientific Instruments, 2021, 92, 043518.	0.6	0
162	Magnetic shear effect on plasma transport at T _e /T _i â^¼ 1 through electron cyclotron heating in DIII-D plasmas. Nuclear Fusion, 2021, 61, 016013.	1.6	0